International Journal of Mechanical, Industrial and Aerospace Sciences
ISSN: 2517-9950
Vol:8, No:11, 2014

Compressive Stresses near Crack Tip Induced by Thermo-Electric Field

Thomas Jin-Chee Liu

***Abstract*—**In this paper, the thermo-electro-structural coupled-field in a cracked metal plate is studied using the finite element analysis. From the computational results, the compressive stresses reveal near the crack tip. This conclusion agrees with the past reference. Furthermore, the compressive condition can retard and stop the crack growth during the Joule heating process.

***Keywords*—**Compressive stress, crack tip, Joule heating, finite element.

I. Introduction

THE past references have reported that the Joule heating effect can induce local compressive thermoelastic stresses and melting area at the crack tip [1]–[6]. The compressive stresses can retard and stop the crack growth during the Joule heating process.

Under very high electric load, the crack tip can melt. Then it can shrink to a crack tip hole during the cooling process [4], [7], [8]. This hole can reduce the high stress and remove the singularity at the crack tip. The crack growth can be stopped. The above phenomenon is illustrated in Fig. 1.

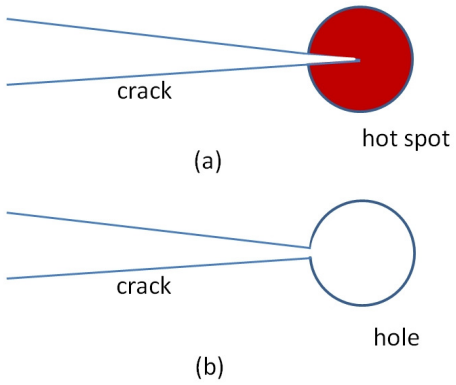

Fig. 1 (a) hot spot at crack tip; (b) crack tip hole

During the heating process, the compressive stresses near the crack tip are important to reduce or stop the potential crack growth. In this paper, this topic is studied by the thermo-electro-structural finite element analyses with the software ANSYS. Based on the author's previous studies [7]–[9], the crack contact condition and temperature-dependent material data are considered in the simulations. The stress, temperature and electric current density fields are obtained for estimating the crack tip behaviors.

Thomas Jin-Chee Liu, Associate Professor, is with the Department of Mechanical Engineering, Ming Chi University of Technology, Taishan, New Taipei City, Taiwan (phone: 886-2-29089899 ext 4569; e-mail: jinchee@mail.mcut.edu.tw).

II. Case Study

Fig. 2 shows the configuration of the case study. A metal plate with a central crack is subjected to the distributed load σ_0 and DC current I_0. This thin plate is made of mild steel with dimensions $2W \times 2L \times e$. The crack length is $2a$.

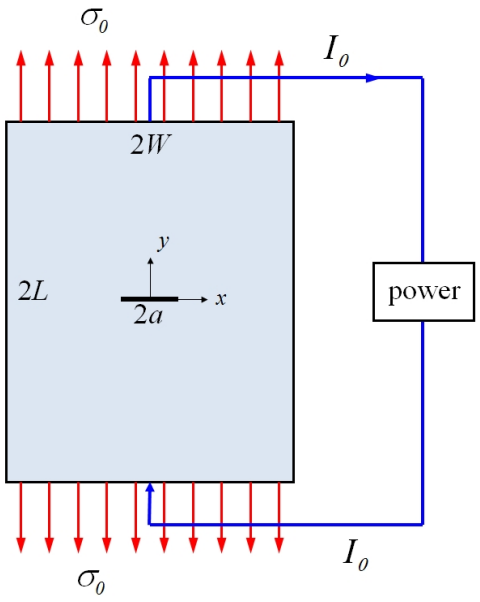

Fig. 2 Configuration and sample

The thermo-electro-structural coupled-field problem in Fig. 2 will be solved by the finite element method. The plane stress, two-dimensional thermo-electric conditions, and isotropic properties are assumed. To simulate more practical conditions, the temperature-dependent material properties in Table I [10] are adopted in the analysis. The electric-current-induced thermo-structural problem is transient. The initial temperature is 21°C. From the conclusion of Liu [8], the phase change effect can be ignored. The convection on all surfaces is also ignored.

The coupled-field contact conditions between crack surfaces are considered in this study. The electric current and heat flow can pass through the crack surfaces when the crack contact occurs. The following equations may describe the electrical and thermal contact conditions [11], [12]:

$$J = \eta_{cel}(\phi_1 - \phi_2) \quad (1)$$

$$q'' = \eta_{cth}(T_1 - T_2) \quad (2)$$

where η_{cel} and η_{cth} are respectively the electrical conductance and thermal conductance of the contact surfaces. The terms $(\phi_1 - \phi_2)$ and $(T_1 - T_2)$ are respectively the electric potential difference and temperature difference between both contact surfaces. In this study, η_{cth} is assumed to be very large so that the thermal contact resistance can be ignored. However, η_{cel} is defined as [12]:

$$\eta_{cel} = \frac{1}{\rho_c l_c} \quad (3)$$

where ρ_c and l_c are the contact resistivity and characteristic length, respectively. For mild steel, the typical values η_{cel} = 6.29×10^8 1/(Ω–m^2), $\rho_c = 6.2586\times10^{-5}$ Ω–m and $l_c = 2.54\times10^{-5}$ m (0.001 inch) [10] are used in ANSYS. In addition, the coefficient of friction on crack surfaces is neglected.

TABLE I
TEMPERATURE-DEPENDENT PROPERTIES OF MILD STEEL [10]

Temperature (°C)	Young's modulus E (GPa)	Yielding strength S_Y (MPa)	Coefficient of thermal expansion α (1/°C)	Thermal conductivity k (W/ m-°C)	Specific heat C_p (J/ kg-°C)	Resistivity ρ (Ω-m)
21	206.8	248	10.98×10^{-6}	64.60	444	0.14224×10^{-6}
93	196.5	238	11.52×10^{-6}	63.15	452.38	0.18644×10^{-6}
204	194.4	224	12.24×10^{-6}	55.24	511.02	0.26670×10^{-6}
315.5	186	200	12.96×10^{-6}	49.87	561.29	0.37592×10^{-6}
426.7	169	173	13.50×10^{-6}	44.79	611.55	0.49530×10^{-6}
537.8	117	145	14.04×10^{-6}	39.71	661.81	0.64770×10^{-6}
648.9	55	76	14.58×10^{-6}	34.86	762.34	0.81788×10^{-6}
760	6.9	14	14.05×10^{-6}	30.46	1005.3	1.0109×10^{-6}
871	–	–	13.05×10^{-6}	28.37	1005.3	1.1151×10^{-6}
982	–	–	–	27.62	1005.3	1.1582×10^{-6}
1093	–	–	–	28.52	1189.6	1.1786×10^{-6}
1204	–	–	–	–	1189.6	1.2090×10^{-6}

* Poisson's ratio ν= 0.3, density β = 7861.2 kg/m^3, melting point = 1521 ºC.

III. METHODS OF ANALYSES

In this study, the finite element equations of the thermo-electro-structural coupled-field analysis are listed as follows [11]:

$$\begin{bmatrix} \mathbf{M} & 0 & 0 \\ 0 & 0 & 0 \\ 0 & 0 & 0 \end{bmatrix} \begin{bmatrix} \ddot{\mathbf{U}} \\ \ddot{\mathbf{T}} \\ \ddot{\mathbf{V}} \end{bmatrix} + \begin{bmatrix} \mathbf{C} & 0 & 0 \\ \mathbf{C}^{\mathbf{tu}} & \mathbf{C}^{\mathbf{t}} & 0 \\ 0 & 0 & 0 \end{bmatrix} \begin{bmatrix} \dot{\mathbf{U}} \\ \dot{\mathbf{T}} \\ \dot{\mathbf{V}} \end{bmatrix} + \begin{bmatrix} \mathbf{K} & \mathbf{K}^{\mathbf{ut}} & 0 \\ 0 & \mathbf{K}^{\mathbf{t}} & 0 \\ 0 & 0 & \mathbf{K}^{\mathbf{v}} \end{bmatrix} \begin{bmatrix} \mathbf{U} \\ \mathbf{T} \\ \mathbf{V} \end{bmatrix} = \begin{bmatrix} \mathbf{F} \\ \mathbf{Q} \\ \mathbf{I} \end{bmatrix} \quad (4)$$

where **U**, **T**, **V**, **F**, **Q** and **I** are the vector forms of the displacement, temperature, electric potential, force, heat flow rate and electric current, respectively. The material constant matrices **M**, **C**, $\mathbf{C}^{\mathbf{t}}$, $\mathbf{C}^{\mathbf{tu}}$, **K**, $\mathbf{K}^{\mathbf{t}}$, $\mathbf{K}^{\mathbf{ut}}$ and $\mathbf{K}^{\mathbf{v}}$ are the structural mass, structural damping, thermal specific heat, thermo-structural damping, structural stiffness, thermal conductivity, thermo-structural stiffness and electric conductivity, respectively. The coupled heat flow matrix **Q** contains the effects of the thermal loading and electrical Joule heating. $\mathbf{C}^{\mathbf{tu}}$ and $\mathbf{K}^{\mathbf{ut}}$ are thermo-structural coupled terms. Equation (4) is a directly coupled nonlinear equation which is solved using the Newton-Raphson iterative method.

The finite element model of the previous study [8] is adopted in this paper. The accuracy of the mesh has been validated by Liu [8]. Fig. 3 shows the finite element mesh of ANSYS with W=L=0.05 m and a=0.01 m. Due to the symmetry of the problem, only a half plate of Fig. 2 is analyzed. The symmetric conditions are applied on the finite element model. The plate is modeled by ANSYS element type: PLANE223, i.e. the 8-node isoparametric plane element with the thermo-electro-structural coupled-field analysis. The plane stress option is used due to the thin thickness (e=0.001 m). In Fig. 3, the model has 1606 elements and 4899 nodes. The quarter-point elements (QPE) [13] are used for modeling the $r^{-1/2}$ singularity at the crack tip.

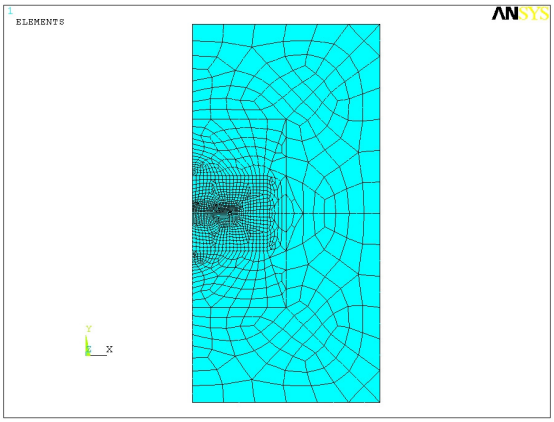

(a)

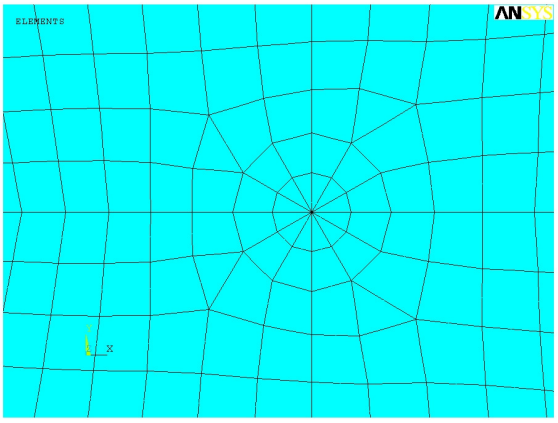

(b)

Fig. 3 Finite element model (a) half model (b) local mesh

IV. Results and Discussions

To investigate the coupled-field on the plate, the electric load I_0=8000 A is applied on the plate boundary. The mechanical load is removed (σ_0=0 Pa). The total operating time is 1 s. In Figs. 4 to 6, the temperature, electric current density and stress fields are obtained and shown.

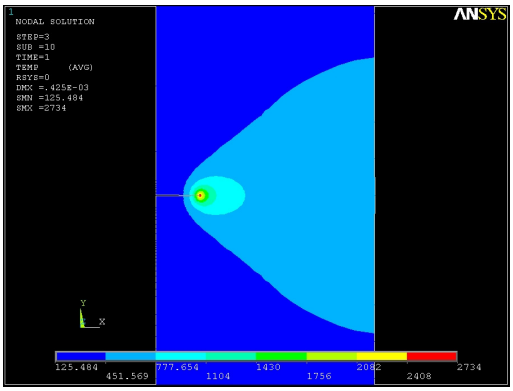

Fig. 4 Temperature field (°C)

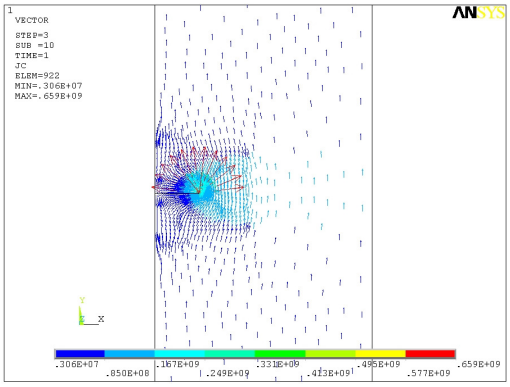

Fig. 5 Electric current density vector field (A/m^2)

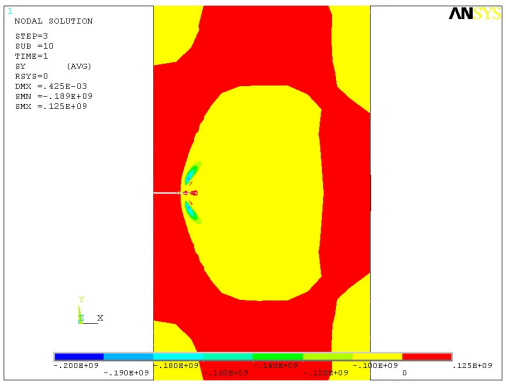

Fig. 6 Stress field (σ_y, Pa)

In Fig. 4, it can be seen that the Joule heating effect causes a hot spot at the crack tip. It demonstrates the existence of the melting crack tip when enough electrical energy is provided. Also, it is noted that there is an electric field concentration at the crack tip (shown in Fig. 5). Similar to the elastic stress field, the electric current density also has the $r^{-1/2}$ singularity at the crack tip [3]. Under the Joule heating effect, this current density concentration induces the hot spot around the crack tip (Fig. 4).

Fig. 6 shows the stress field of σ_y. In front to the crack tip, there is a large area associated with negative stress values. In other words, the compressive stresses occur in this area.

In Fig. 7, it shows the distribution of σ_y along the line in front to the crack tip. Also, it reveals a large region which has the compressive stresses. In Fig. 8, it shows the time-history of σ_y at a node near the crack tip. It has compressive stress state during 0 ~ 1 s.

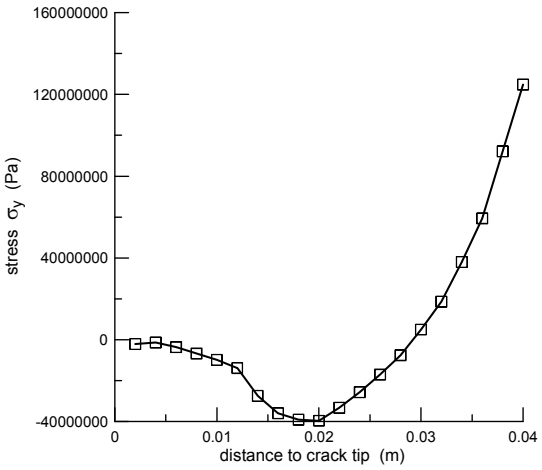

Fig. 7 Stress distribution of σ_y

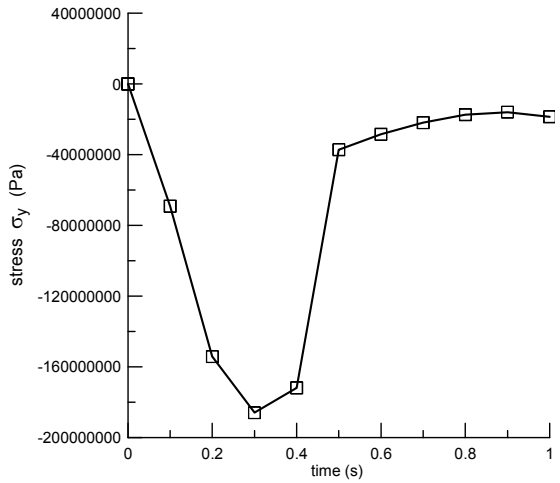

Fig. 8 Time-history of σ_y

V. Conclusions

From the computational results, the compressive stresses reveal near the crack tip. This conclusion agrees with the past studies. Furthermore, the compressive condition can retard and stop the crack growth during the Joule heating process.

References

[1] Kudryavtsev BA, Parton VZ and Rubinskii BD. Electromagnetic and thermoelastic fields in a conducting plate with a cut of finite length. Solids. Mech. 17, pp. 110–118, 1982.
[2] Parton VZ and Kudryavtsev BA. Electromagnetoelasticity. Gordon and Breach, New York, 1988.
[3] Cai GX and Yuan FG. Electric current-induced stresses at the crack tip in conductors. Int. J. Fract. 96, pp. 279–301, 1999.
[4] Fu YM, Bai XZ, Qiao GY, Hu YD and Luan JY. Technique for producing crack arrest by electromagnetic heating. Mater. Sci. Tech. 17, pp. 1653–1656, 2001.
[5] Hasanyan D, Librescu L, Qin Z and Young RD. Thermoelastic cracked plates carrying nonstationary electrical current. J. Therm. Stress. 28, pp. 729–745, 2005.
[6] Qin Z, Librescu L and Hasanyan D. Joule heating and its implications on crack detection/arrest in electrically conductive circular cylindrical shells. J. Therm. Stress. 30, pp. 623−637, 2007.
[7] Liu TJC. Thermo-electro-structural coupled analyses of crack arrest by Joule heating. Theor. Appl. Fract. Mech. 49, pp. 171–184, 2008.
[8] Liu TJC. Finite element modeling of melting crack tip under thermo-electric Joule heating. Engng. Fract. Mech. 78, pp. 666684, 2011.
[9] Liu TJC. Fracture mechanics of steel plate under Joule heating analyzed by energy density criterion. Theor. Appl. Fract. Mech. 56, pp. 154161, 2011.
[10] Tsai CL, Dai WL, Dickinson DW and Papritan JC. Analysis and development of a real-time control methodology in resistance spot welding. Weld. J. 70, pp. s339–351, 1991.
[11] ANSYS HTML online documentation. SAS IP, Inc., USA, 2005.
[12] Sun X and Dong P. Analysis of aluminum resistance spot welding processes using coupled finite element procedures. Weld. J. 79, pp. s215s221, 2000.
[13] Barsoum RS. On the use of isoparametric finite elements in linear fracture mechanics. Int. J. Numer. Meth. Eng. 10, pp. 2537, 1976.